ELSEVIER

Earth and Planetary Science Letters 133 (1995) 35–46

EPSL

Distribution of shortening between the Indian and Australian plates in the central Indian Ocean

James Van Orman [a,b], James R. Cochran [a], Jeffrey K. Weissel [a], Florence Jestin [c]

[a] *Lamont-Doherty Earth Observatory of Columbia University, Palisades, NY 10964, USA*
[b] *Department of Geology, Florida State University, Tallahassee, FL 32306, USA*
[c] *Laboratoire de Géologie, CNRS URA 1316, Ecole Normale Supérieure, 24 rue Lhomond, 75231 Paris Cedex, France*

Received 4 May 1994; accepted 28 March 1995

Abstract

We analyze a single-channel seismic (SCS) reflection profile that completely crosses the zone of deformed oceanic lithosphere in the central Indian Ocean at 78.8° E. By summing the apparent shortening on all seismically resolvable faults (throws $> \sim 10$ m), we find that 11.2 ± 2 km of shortening has occurred at this longitude during the past 7.5 m.y. This estimate, together with the 27 ± 5 km of shortening previously estimated from a multichannel seismic (MCS) profile farther east at 81.5° E, are consistent with the west-to-east increase in shortening predicted by Euler poles which treat the Indian and Australian plates as separate tectonic units. Our result therefore provides direct evidence from the deformation itself that the compression of oceanic lithosphere in the central Indian Ocean, originally regarded as 'intraplate', is better described as constituting part of a broad boundary zone between distinct Indian and Australian plates.

We also examine the size statistics of faults revealed in SCS and MCS profiles running nearly normal to the deformation trends in the longitude band 78.8° E–81.5° E. The N–S extent of the deformation does not change appreciably over these longitudes. We find that the average fault spacing remains constant at about 7 km, whereas the mean throw increases systematically from west to east (~ 74 m to ~ 177 m). Basically the contribution of 'small' faults (those with throws of 10–50 m) decreases systematically across the deforming region (i.e., with increasing amount of shortening). This suggests that the deformation occurs by reactivation of a select fault population, that these faults continue to add displacement with time and that relatively few new faults are initiated. We also infer from the fault size statistics that the contribution to the deformation of faults below the resolution of the seismic methods (~ 10 m for SCS and ~ 50 m for MCS) is likely to be quite limited.

1. Introduction

Plate tectonics rests on the assumption that lithospheric plates in relative motion on the Earth's surface are rigid except at their boundaries. The rigidity assumption is important because it implies that deformation is restricted to plate boundaries and that plate interiors remain basically undeformed. This allows the determination of present-day plate velocities and reconstruction of various continental fragments through time in a simple fashion. The assumption that lithospheric plates are internally rigid generally appears to be justified. However, abundant evidence has emerged of a broad zone of deformation extending eastward across the equatorial Indian Ocean from the Chagos–Laccadive Ridge to beyond the Ninetyeast Ridge in a region that was originally considered to be within the Indo-Australian plate [1].

Elsevier Science B.V.
SSDI 0012-821X(95)00061-5

Evidence for deformation consists of seismicity [2–8], seismic reflection, heat flow and marine gravity data [9–13] and characteristic lineated long-wavelength gravity and geoid anomalies derived from satellite altimetry [10,14–16].

Although the extent of the region involved in the deformation depends to some degree on the type of geophysical observations used to define tectonic activity [10,17], all workers agree that deformation in response to N–S directed compression has occurred in the equatorial Indian Ocean to the east of 78° E extending at least to the Ninetyeast Ridge (Fig. 1). The lithospheric deformation began in the Late Miocene (7–8 Ma) according to ODP Leg 116 drilling results [18,19]. The actual regional extent and mode of deformation westward across the Chagos–Laccadive Ridge and eastward across the Ninetyeast Ridge into the Wharton Basin, however, remains the subject of discussion (e.g., [16,17,20,21]).

Although the deformation in the central Indian Ocean has been widely referred to as 'intraplate', Wiens et al. [22] argued that it is more appropriate to consider it as forming a diffuse, but distinct, plate boundary between separate Indian and Australian plates rather than occurring within the interior of a single Indo-Australian plate and determined a pole for this motion. DeMets et al. [17,22–25] have subsequently worked to further demonstrate that plate motion data along the Indian Ocean spreading ridges preclude a single rigid Indo-Australian plate and to

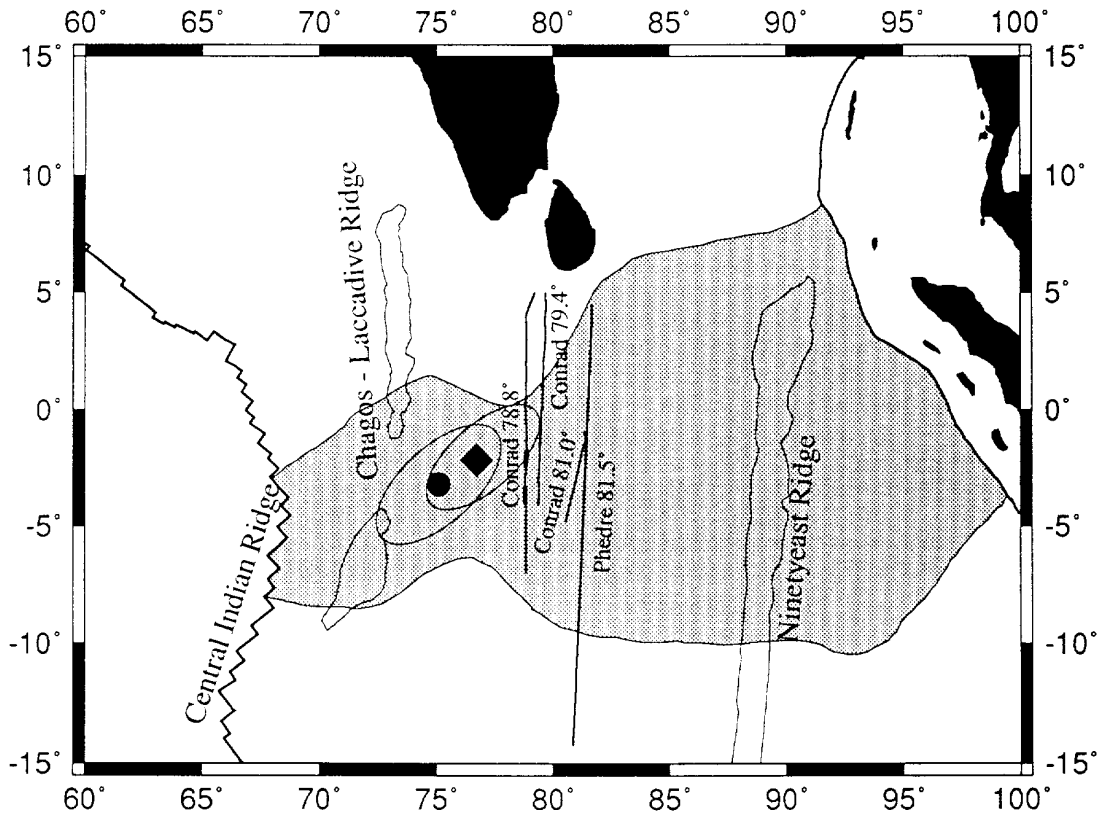

Fig. 1. Location map of the central Indian Ocean showing location of seismic lines discussed in this study together with recognized plate boundaries and major bathymetric features. Shaded area shows the region of deformation extending through the central Indian Ocean as defined by Gordon et al. [17]. ● = Location of Indian–Australian Euler pole determined by DeMets et al. [24] for motion since Anomaly 2A (3 Ma); ♦ = location of Anomaly 5 (~ 10 Ma) pole determined by Royer et al. [26]. Standard error ellipses are shown for both poles. Portions of the *Conrad* line at 78.8° E shown in Fig. 2 are indicated with heavier lines.

better constrain an Euler pole describing motion between independent Indian and Australian plates. These studies used transform fault azimuths, earthquake slip vectors and spreading rates since the middle of Anomaly 2A (~ 3 Ma) from the Carlsberg, Central Indian and Southeast Indian ridges. Their most recent solution [24] places the pole at 3.2° S, 75.1° E with a rotation rate of 0.305°/m.y. This pole describes the average motion between the Indian and Australian plates over the past 3 m.y. DeMets et al. [24] also concluded that a triple junction between the Indian, Australian and African plates is located at 8° S–9° S on the Central Indian Ridge near the Vema fracture zone.

Recently, Royer et al. [26] proposed that Anomaly 5 magnetic anomaly data could best be fit by an Australia/India pole at 2.1° S, 76.7° E with a total rotation of 2.15°. This pole is located very close to the pole determined by DeMets et al. [24]. If the deformation is considered to have begun at 7.5 Ma [19], the two poles also agree well in rotation rate. Given the uncertainties inherent in determining rotation poles from magnetic anomaly data, these poles are essentially identical.

However, because the rotation pole is so close to (actually within) the deformed region, a small error in its position results in large changes in the amount, distribution and direction of motion between the plates. At 78.8° E (the location of the seismic profile analyzed in this paper), the shortening predicted by the DeMets et al. [24] and Royer et al. [26] poles varies by 72% (16.4 km vs. 9.5 km). The shortening calculated from the two poles varies by 52% at 80° E (21.7 km vs. 14.3 km) and by 19% at 90° E (65.3 km vs. 55.1 km). These significant differences exist even though the two poles are located within each other's 95% confidence limits. However, an important and testable prediction of both of these poles is that there should be a very significant and systematic west to east increase in the amount of shortening across the central Indian Ocean.

An additional complication comes from the fact that motion on a sphere occurs along small circles centered on the Euler pole. Since the poles determined from plate motion data are so close to the deforming area, this means that the predicted convergence direction varies significantly within the deforming region. At 78.8° E, the longitude of the seismic profile discussed in this study, the DeMets et al. [24] pole predicts N–S convergence at 3.2° S, directly east of the pole. It also predicts N41° W convergence at the equator in the northern portion of the deforming region and N37° E convergence at 6° S in the southern portion. The total variation in the convergence direction across the deforming area at that latitude is therefore 78°, rotating from NE–SW in the south to NW–SE in the north. Wherever it has been possible to determine the trend of the faults accommodating crustal shortening, the faults consistently trend at 90–100° independent of the latitude [11,12,27]. There is little evidence of strike-slip motion on the faults. In addition the N–S trending fracture zones in the Central Indian Basin are not offset or reactivated by the recent deformation and show no sign of either compressional or extensional deformation [12,13,29]. Thus, it appears that shortening has been in a nearly N–S direction throughout the deforming area. This observation appears to conflict with interpretation of the broad zone of deformation strictly as a wide plate boundary.

Most previous estimates of the amount and distribution of shortening in the central Indian Ocean [24,26] are based on inversions of magnetic anomaly data, transform azimuths and slip vectors from mid-ocean ridge earthquakes. They are thus not direct determinations or measurements, but are predictions based on a model of plate boundary data. Seismic reflection profiling provides an independent method of determining the total shortening across the deformed zone. The fault geometry is revealed on seismic reflection lines. If seismic images of the faults and the manner in which they offset markers in the sediments and/or crust can be used to determine the shortening on the faults, a direct measurement of the total amount of shortening can be obtained by summing the contribution of all faults on a transect across the deformed zone. At least two profiles are needed to test the concept of a broad but distinct plate boundary because, as mentioned above, one of the important predictions of the kinematic analyses [24,26] is that the amount of convergence increases rapidly and systematically across the central Indian Ocean.

A number of seismic reflection surveys have been conducted in the Central Indian Basin [9–13,28]. However, very few profiles capture the entire N–S

extent of the deformation. One shortening estimate from a single multichannel seismic (MCS) line spanning the deformed zone along 81.5° E obtained during the *Phèdre* cruise of the French vessel *Marion Dufresne* has been published by Chamot-Rooke et al. [29]. They determined that the contribution of

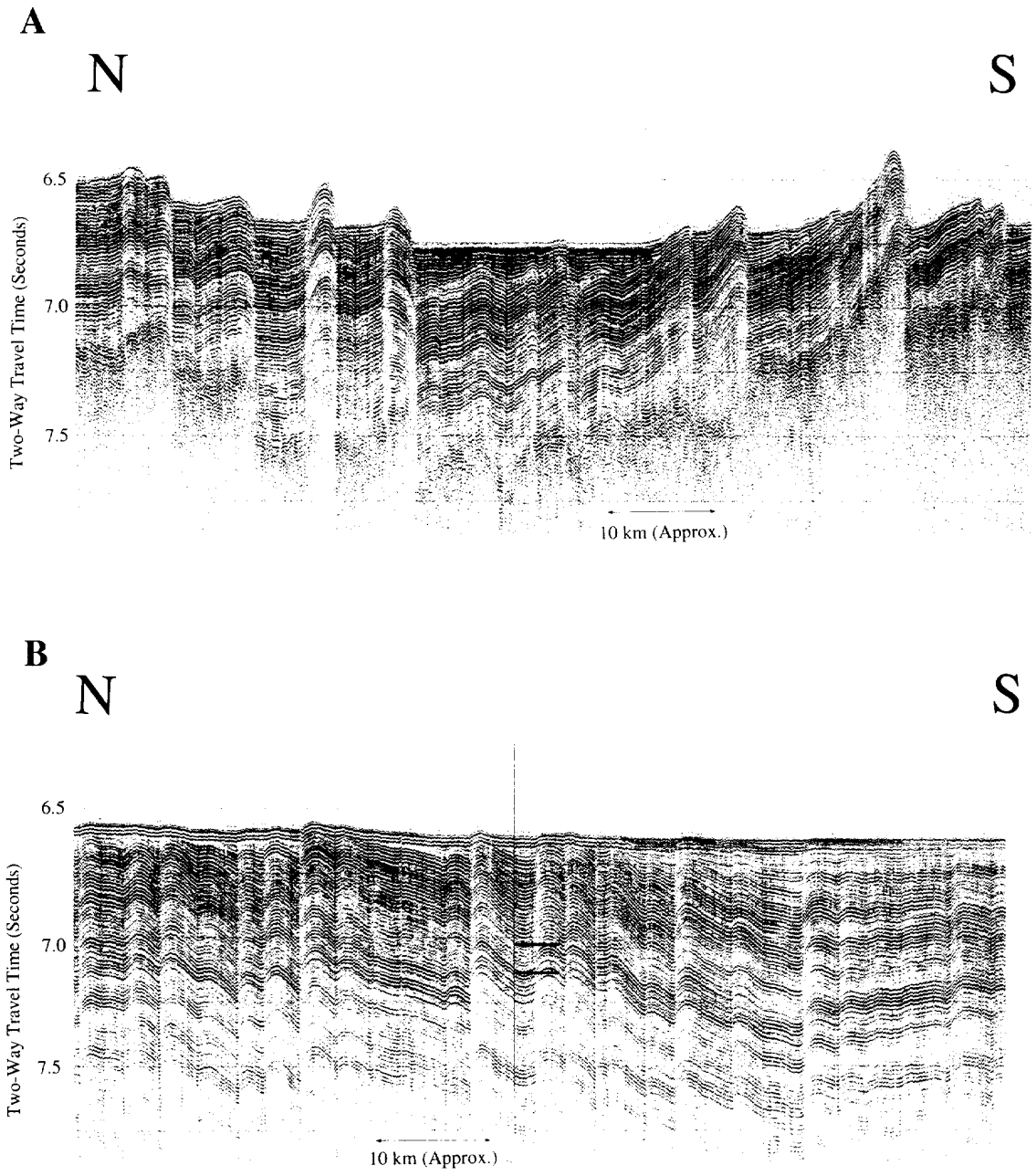

seismically resolvable faults amounts to 22–37 km of shortening (depending on the assumed dip angle and whether the faults are assumed to be planar or listric) distributed over a zone of deformation 900 km in N–S extent.

This paper presents a critical second estimate of shortening from a single-channel seismic (SCS) line that also completely crosses the deformed area. This line was obtained on R.V. *Robert D. Conrad* cruise 2707 along 78.8° E, about 300 km to the west of the *Phèdre* line. The Conrad seismic line not only gives a second estimate of the shortening across the deformed region, but also is located far enough to the west of the *Phèdre* line to allow us to test whether there is a west-to-east increase in the amount of shortening as predicted by rotation about a stable Euler pole similar to the poles determined by DeMets et al. [24] and Royer et al. [26].

A second *Conrad* seismic profile at 81° E which spans only part of the deformed zone was also analyzed to compare with the nearby *Phèdre* line in order to investigate whether shortening estimates obtained from SCS and MCS profiles are equivalent. A third profile, also a partial crossing, collected at 79.4° E, allows us to examine latitudinal changes in the style of faulting and to give some measure of the small-scale west-to-east variability in shortening.

2. Method of obtaining shortening estimates

Compressional deformation in the central Indian Ocean occurs on two distinct spatial scales or wavelengths. At long wavelengths, the surface of the oceanic crust and most of the overlying Bengal Fan sediment cover is deformed into broad E–W trending undulations with wavelengths of 100–300 km and peak-to-trough amplitudes of 1–3 km [10–12,28,29]. Large-amplitude gravity and geoid anomalies correlate with the broad basement deformation features [10,15]. At short wavelengths, seismic reflection profiles show that the oceanic crust is broken into fault blocks bounded by high-angle reverse faults spaced 5–20 km apart [9–13].

We consider here only the shortening resulting from faulting. We assume that shortening estimated from faulting is representative of shortening across the entire lithospheric thickness. The contribution of the long-wavelength basement undulations is quite small [11,17,30]. The strain resulting from deformation of the lithosphere into sinusoids with an amplitude and wavelength characteristic of the observed deformation is less than 10^{-3}, and Gordon et al. [17] estimate that the folding results in only about 0.1–1.5 km of shortening across the deformed region.

The horizontal offset on the faults cannot be resolved on seismic profiles (Fig. 2). We thus determined the shortening by measuring the vertical offset on faults and applying reasonable constraints on the geometry of the faults. Vertical offsets of as little as 0.01 s two-way travel time (twtt) or ~ 10 m could be identified on our high-resolution seismic lines (Fig. 2), compared with an approximately 50 m resolution for the *Phèdre* lines [29]. Bull and Scrutton [13] demonstrated that shortening in the sediments is accommodated by a combination of folding and faulting. As a result the offset of a reflector right at the fault is not a good measure of the vertical offset (throw). We thus estimated the throw of each fault by determining the maximum offset of reflectors, which can occur up to 1 km from the fault (Fig. 2). The throw across each individual fault identified on the seismic lines was measured in twtt directly from the seismic reflection profile (Fig. 2). In order to avoid uncertainties resulting from initial basement relief and syndeformational sedimentation, all fault offsets were measured above the sediment/basement interface, but below the prominent Upper Miocene unconformity that marks the onset of deformation [19,31]. We were also careful to use distinctive

Fig. 2. Representative portions of the single-channel seismic (SCS) line across the deforming region at 78.8° E collected on R.V. *Robert D. Conrad* cruise 2707. Section A extends from 3° 16′S to 4° 02′S and shows a region of relatively large faults. Section B extends from 1° 43′S to 2° 27′S and shows a region of less intense deformation. The location of both sections is indicated on Fig. 1. Vertical exageration in the sediments is about 18:1. North is to the left on both sections. An example of how throw on the faults was measured is shown in Section B. The two heavy horizontal lines show the depth to the same characteristic set of reflectors to the south (top line) and north (bottom line) of a fault. The distance between these two lines gives the vertical throw of the fault in seconds. Note that the offset is not measured exactly at the fault since folding also occurs near the faults.

sequences of reflectors to measure the vertical offset in order to be confident of our correlations across the faults. If the correlation is one cycle off, the resulting error would be no more than 10 to a few tens of meters for the frequencies recorded in the SCS data. Such errors will be of both signs and should average to zero over the length of the profile.

Fault offsets were converted from twtt to vertical distance using a velocity–depth relationship determined for the area around the ODP Leg 116 drill sites (fig. 4 in [32]). It was assumed that sedimentary reflectors in this interval were flat and horizontal prior to faulting [27], so that vertical offset of the sedimentary reflectors represents the vertical offset of the crust during deformation. If we know the dip angle of the crustal faults, the vertical offsets can be easily turned into horizontal crustal shortening. This technique, which is the same as that used by Chamot-Rooke et al. [29], is completely independent of the dip of the faults in the sedimentary column.

Bull and Scrutton [12,13] determined an average dip of about 40° for crustal faults observed on their MCS reflection lines, whose locations bracket those of our SCS profiles. Chamot-Rooke et al. [29] calculated mean dips for crustal faults of 36–45° for assumed crustal velocities of 5–7 km/s. We will therefore assume an average dip of 40° on planar faults for all shortening estimates presented here, both for the *Conrad* lines and the *Phèdre* line. The shortening estimates would increase by about 30% if listric fault geometries were assumed. Our shortening estimates also assume that the seismic lines were run perpendicular to the faults, which appears to be the case. If the ship tracks diverged as much as 20° from the normal to the strike of the faults, the fault dip would be underestimated slightly and the resulting shortening would be overestimated by about 6%.

3. Results

A total of 127 faults were observed on the primary *Conrad* line along 78.8° E between 0.8° N and 6.6° S. The zone of shortening is thus 823 km in N–S extent on this profile. Note that faulting observed on the seismic line does not extend as far south as the shaded region in Fig. 1, which is taken from Gordon et al. [17]. The map in Fig. 1 is based primarily on earthquake epicenter locations and lineated gravity anomalies determined from satellite

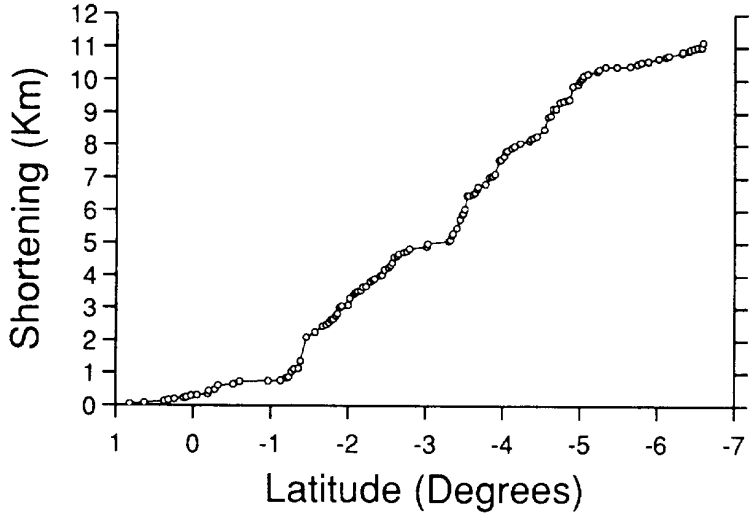

Fig. 3. Plot of the cumulative shortening measured on the *Conrad* seismic line at 78.8° E. ○ = Location of faults observed on the seismic line. The total measured shortening along the 78.8° E transect, assuming planar faults dipping at 40°, is 11.2 km. Note that deformation is concentrated in the central portion of the deforming region between 1.5° S and 5° S and dies away to the north and south. See Fig. 1 for location of seismic lines.

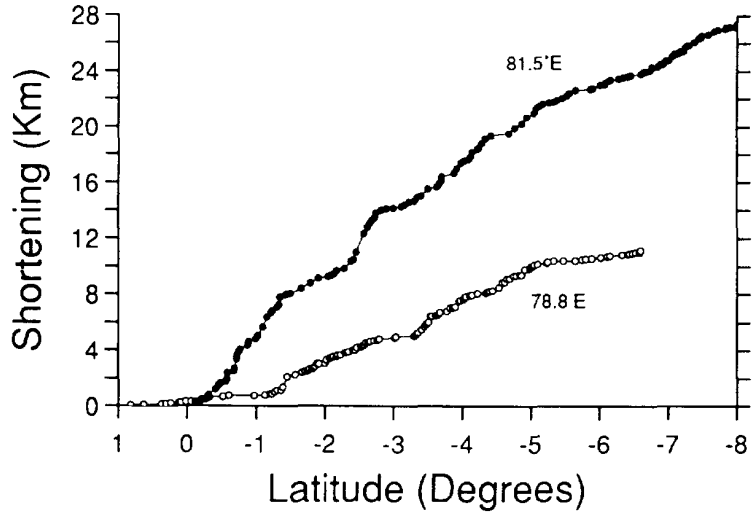

Fig. 4. Comparison of the cumulative shortening measured on the *Phédre* seismic line at 81.5° E (●) and on the *Conrad* line at 78.8° E (○). Planar faults dipping at 40° are assumed in calculating shortening on the faults in both cases.

altimetry. Similarly, faulting is only observed from just north of the equator to 8° S on the *Phèdre* line at 81.5° E [29], which is also somewhat less than the extent of the shaded region in Fig. 1.

The vertical offset on faults observed on the 78.8° E *Conrad* seismic line ranged from 9 to 623 m with a mean throw of 73.3 m. A cumulative shortening curve for the line is shown in Fig. 3. Subhorizontal sections can be seen at both ends of the curve, graphically illustrating the fading away of the defor-

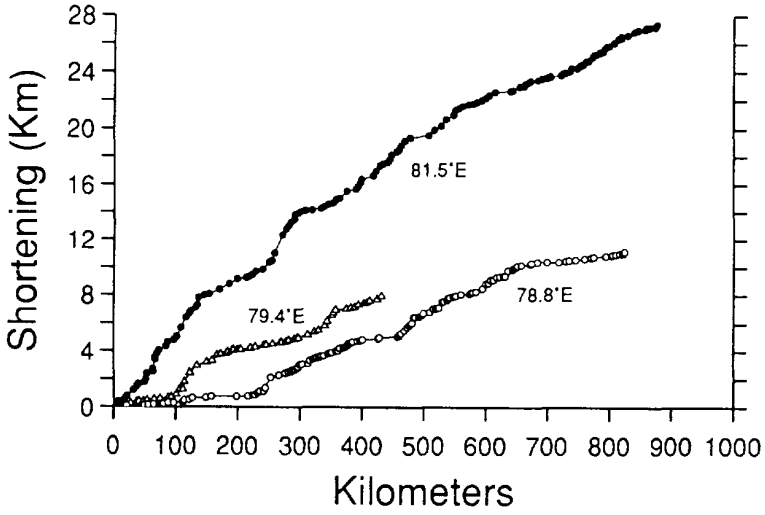

Fig. 5. Comparison of the cumulative shortening measured on the *Phédre* seismic line at 81.5° E (●) and the Conrad seismic lines at 78.8° E (○) and 79.4° E (△). The curves are aligned on the northernmost fault observed on each seismic line which is placed at 0 km on the horizontal axis. The *Conrad* 79.4° E line does not extend to the southern limit of the deformation. Note the regular eastward increase in crustal shortening..

mation at both the north and south ends of the main zone of shortening. The central portion of the cumulative curve is approximately linear, demonstrating a relatively constant N–S distribution of shortening between 1.5° S and 5° S. The total measured shortening along the 78.8° E transect, assuming planar faults dipping at 40°, is 11.2 km. Thus the shortening factor across the zone of faulting is about 1.4%.

The shortening measured on the *Conrad* line at 78.8° E is considerably less than the estimate of 27.4 km (shortening factor = 3.1%) obtained from the *Phèdre* dataset at 81.5° E (Fig. 4). Fig. 5 shows cumulative shortening curves for the three seismic lines that cross the northern end of the deformed region. The seismic line at 79.4° E does not reach the southern end of the deformation. These cumulative shortening curves clearly demonstrate the systematic eastward increase in crustal shortening. The two shortening estimates obtained from seismic lines that cross the entire deformed region are compared in Fig. 6 with the shortening predicted by the DeMets et al. [24] and the Royer et al [26] Euler poles assuming that motion started at 7.5 Ma [19]. The shortening increases systematically from west to east away from the pole position and agrees well with that predicted by the DeMets et al. [24] and Royer et al. [26] poles at both locations within the uncertainties of the measurements. The shortening data taken by themselves suggest that the total motion pole may be slightly to the east the poles determined by DeMets

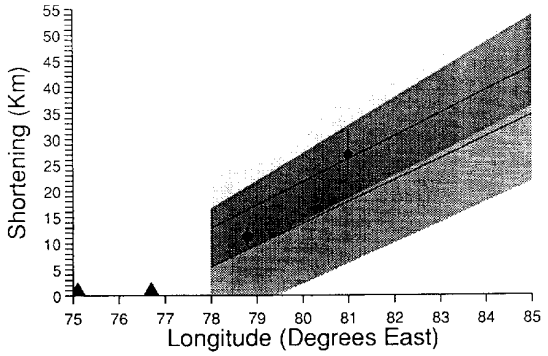

Fig. 6. Observed shortening in the central Indian Ocean determined from seismic reflection profiles compared with shortening predicted by the Euler poles proposed by DeMets et al. [24] (upper solid line) and by Royer et al. [26] (lower solid line) along N–S lines as a function of longitude. Longitude of poles is shown by triangles (▲). Light gray and medium gray areas show a range of possible values for, respectively, the DeMets et al. and Royer et al. poles given the uncertainty in the pole positions. (Dark grey area is overlap of the two regions.) Dots (●) show shortening estimate for planar faults dipping at 40° and vertical bars show range for faults dipping at 36–45°. The observed eastward increase in shortening is compatible with both estimates of the pole position.

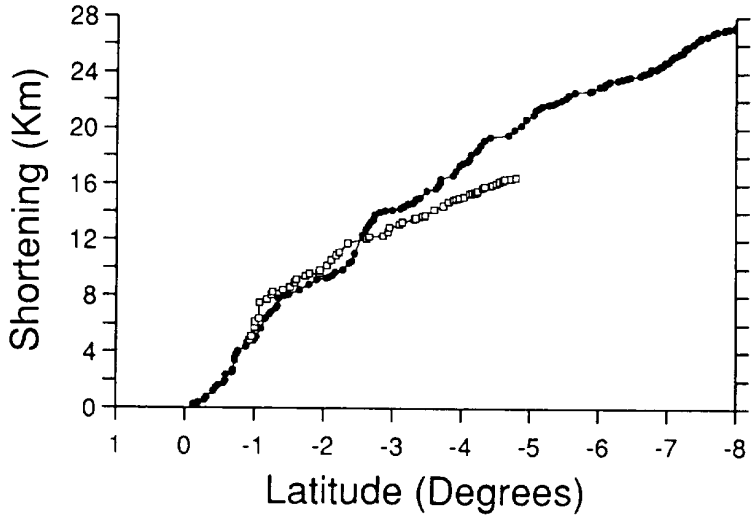

Fig. 7. Comparison of shortening determined from the *Phédre* multichannel seismic (MSC) line at 81.5° E (●) and the *Conrad* SCS seismic line at 81° E (□). The *Conrad* line does not cross either the northern or southern boundaries of the deformed region. It has been adjusted vertically to coincide with the *Phédre* line at its northern end.

et al. [24] and Royer et al. [26] and have a slightly higher angular rotation rate. However, it is clear from these results that the Indian and Australian plates can be considered as separate, distinct entities which have moved relative to each other about a relatively stable pole position since 7.5 Ma.

The cumulative shortening measured on the *Conrad* profile which crosses part of the deformed area at 81° E is approximately 3.4 km less than on the equivalent section of the *Phèdre* line at 81.5° E (Fig. 7). This is greater than the difference in shortening of 2–2.3 km expected across the entire deforming region at these two locations due to the difference in the distance from the pole of the two profiles [24,26] (Fig. 6). It is possible that the discrepancy between the shortening estimates from the two lines is simply a consequence of local variations in the N–S distribution of shortening within the deforming region. Such a lateral variation in the distribution of shortening is evident in Fig. 7 from the observation that between 0.9° S and 2.4° S there is actually 2.4 km more shortening on the *Conrad* SCS line at 81° E than on the *Phèdre* MCS line at 81.5° E.

On the other hand, the discrepancy between the shortening determined on these two reasonably close profiles may result from differences in the resolution of SCS and MCS data or perhaps simply from the fact that the two seismic records were analyzed by different people. If the difference between the estimates obtained from the *Conrad* profile at 81° E and the *Phèdre* line at 81.5° E represents the uncertainty in the method, then the uncertainty can be estimated at about 15–20%. Even if the uncertainty is that large, it is still much less than the difference in shortening recorded on the 78.8° E *Conrad* profile and the *Phèdre* line, and does not affect the conclusions of this study.

4. Discussion

The lower limit of resolution of fault offsets on the *Phèdre* MCS seismic reflection line is about 50 m [29], whereas we can resolve offsets as small as about 10 m on the *Conrad* SCS lines. The contribu-

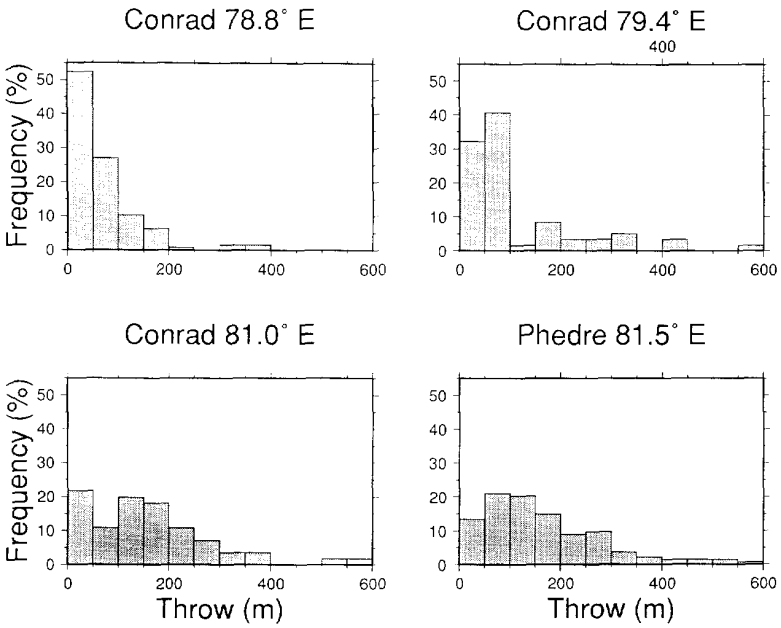

Fig. 8. Histograms of the throw on faults observed on seismic reflection profiles across the deforming region of the central Indian Ocean. Note the systematic change in distribution of fault throw from west to east. Faults with small throw (< 50 m) predominate in the west. Moving to the east, the distribution shifts progressively toward faults with greater throw.

tion of faults with throws of 10–50 m on the three *Conrad* lines is 16.1% of the total measured shortening at 78.8° E, 8.5% at 79.4° E, and 4.1% at 81° E. The observation that the contribution of small faults (throw of 10–50 m) decreases systematically from west to east across the deforming region is reflected in the observation that the distribution of measured throws on the faults steadily shifts toward larger throws from west to east across the central Indian Ocean (Fig. 8). The mean throw on the faults increases from 73.7 m at 78.8° E to 113.5 m at 79.4° E and to 177.6 m at 81° E. An eastward increase in the mean throw is required by the fact that the deforming region does not broaden significantly to the east across these longitudes and that the mean spacing of the faults remains relatively constant across the region (6.53 ± 5.82 km at 78.8° E, 7.43 ± 3.90 km at 79.4° E and 7.80 ± 5.94 km at 81° E). Shortening in the central Indian Ocean appears to be occurring through reactivation of pre-existing faults bounding the abyssal hills [13,15]. Thus the increased shortening toward the east is accommodated by more displacement on these active faults rather than by creation or reactivation of additional faults.

It is necessary to consider how much shortening is accommodated by faults with small offsets below the resolution of the seismic profiles and is thus missed in our analysis. The importance of small-scale faulting in determining total regional strain has been the subject of debate, with estimates of the contribution of small faults (unresolvable in seismic surveys) ranging from negligible [33] to as much as 40% of the total shortening [34]. Cumulative frequency plots of fault offset for the *Conrad* profiles and for the

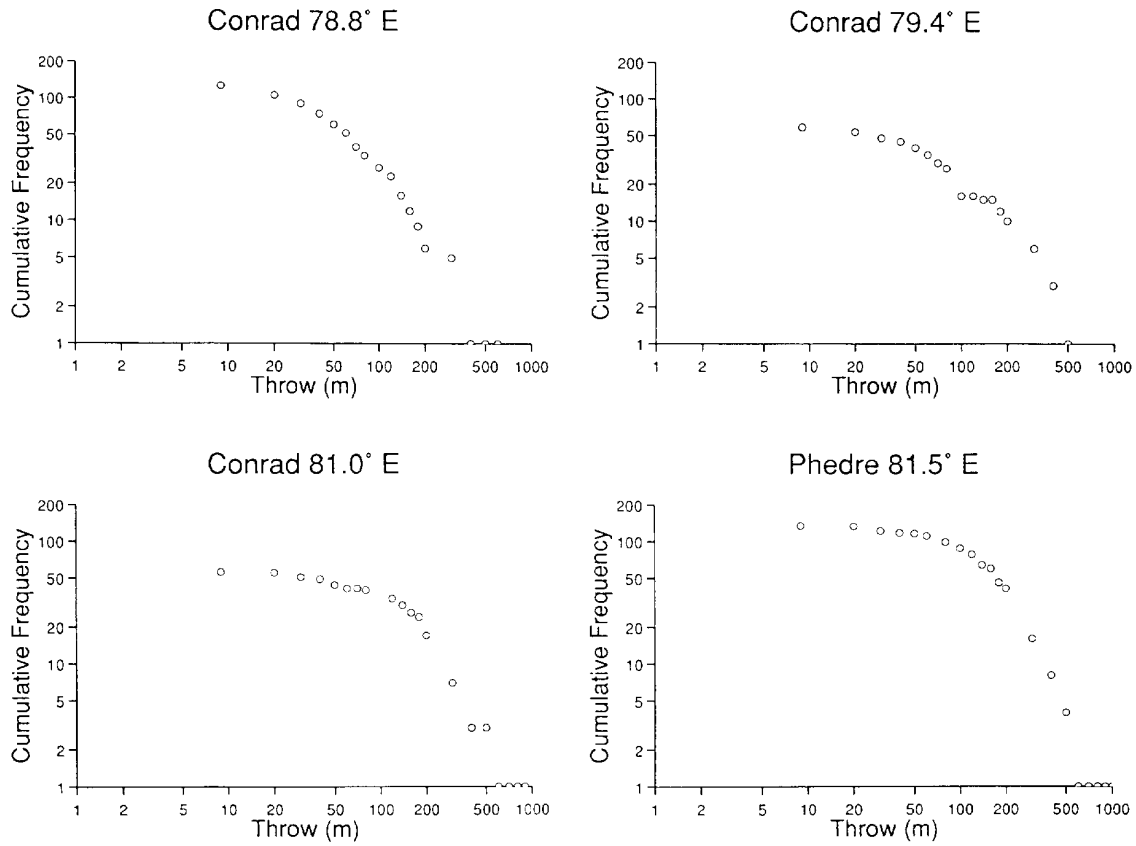

Fig. 9. Plot of log of cumulative frequency against log of vertical throw on faults for seismic reflection lines across the deforming region of the central Indian Ocean.

Phèdre profile are shown in Fig. 9. All of the cumulative frequency plots deviate from a straight line and no simple power-law relationship can be observed in the data. Bull and Scrutton [13] obtained a similar result from their dataset. The deviation of the cumulative frequency plots from a simple power-law relationship makes it difficult to estimate the contribution of very small faults to the total finite shortening reliably. There are fewer small displacement faults observed than predicted from a simple power-law relationship. This could be due either to there being few small displacement faults or to an inability to resolve all of the small faults on the seismic lines.

An important consideration in estimating the contribution of unresolved small faults is whether faulting actually does occur on all scales or whether there is a lower limit on the displacement or spacing of faults which serves to limit the contribution of small faults. There are three observations that suggest that the contribution of small faults is small. These are the fact that as the shortening increases to the east the average fault spacing remains constant, the deformed zone does not widen appreciably, and the percentage of observed faults on the *Conrad* lines with less than 50 m of throw decreases from 52% at 78.8° E to 21% at 81° E. Taken together, these observations imply that the increased shortening toward the east is taken up by increased throw on similar fault populations. Thus while a large number of faults with 10–50 m of throw acquired more than 50 m of throw in moving from the amount of total shortening at 78.8° E to that at 81° E, there were far fewer small faults which acquired 10 m of throw and thus became resolvable. Thus, although our shortening measurements must be treated as minimum estimates, the contribution to the total shortening by faults below the resolution of our seismic records (i.e., those with less than $\sim$ 10 m of vertical offset) is likely to be quite limited.

5. Summary and conclusions

The total shortening observed across the deformed region of the central Indian Ocean along a N–S single-channel seismic reflection transect at 78.8° E amounts to 11.2 ± 2 km (a shortening factor of 1.4%). This is considerably less than the estimate of 27 ± 5 km (shortening factor of 3.1%) obtained from a multi-channel seismic line farther east at 81.5° E [29]. These two shortening estimates are consistent with convergence between the regions on either side of the deformed region since 7.5 Ma about an Euler pole similar to the pole determined by DeMets et al. [24] for motions during the past 3 m.y. and by Royer et al. [26] for the past 10 m.y. The fact that the total shortening measured from seismic lines can be described by the same Euler pole over a period of 7.5 m.y. supports the concept that the deformed region in the central Indian Ocean is best considered as a broad plate boundary zone separating distinct, independent and well-defined Indian and Australian plates, rather than as a zone of intraplate deformation as originally believed.

Fault spacing remains relatively constant from west to east across the deformed region, consistent with the conclusion that the shortening occurs by reactivation of old normal faults forming the abyssal hill fabric of the oceanic crust [10,12]. Since the zone of deformation does not broaden substantially from 78.8° E to 81.5° E, much of the increase in shortening must be accommodated by an increase in the throw of individual faults. The mean throw on faults observed on the three *Conrad* lines increases monotonically to the east from 73.7 m at 78.8° E to 177.6 m at 81° E.

Acknowledgements

This research was supported by National Science Foundation grant OCE 92-04168. J.V.O. participated in this work as part of an undergraduate summer internship program supported by NSF grant OCE 92-00116. We thank Roger Scrutton and two anonymous reviewers for helpful comments and suggestions. This is Lamont-Doherty contribution 5364. [*MK*]

References

[1] D.P. McKenzie and J.G. Sclater, The evolution of the Indian Ocean since the Late Cretaceous, Geophys. J. R. Astron. Soc. 25, 437–528, 1971.

[2] L.R. Sykes, Seismicity of the Indian Ocean and a possible

nascent island arc between Ceylon and Australia, J. Geophys. Res. 75, 5041–5055, 1970.
[3] T.J. Fitch, M.H. Worthington and I.V. Everingham, Mechanisms of Australian earthquakes and contemporary stress in the Indian Ocean Plate, Earth Planet Sci. Lett. 18, 345–356, 1973.
[4] S. Stein and E.A. Okal, Seismicity and the tectonics of the Ninetyeast Ridge area: Evidence for internal deformation of the Indian plate, J. Geophys. Res. 83, 2233–2246, 1978.
[5] E.A. Bergman and S.C. Solomon, Oceanic intraplate earthquakes: Implications for local and regional intraplate stress, J. Geophys. Res. 85, 5389–5410, 1980.
[6] E.A. Bergman and S.C. Solomon, Earthquake source mechanisms from body-waveform inversion and intraplate tectonics in the northern Indian Ocean, Phys. Earth Planet. Inter. 40, 1–23, 1985.
[7] D.A. Wiens, Historical seismicity near Chagos: A complex deformation zone in the equatorial Indian Ocean, Earth Planet. Sci Lett. 76, 350–360, 1986.
[8] D.E. Petroy and D.A. Wiens, Historical seismicity and implications for diffuse plate convergence in the northeast Indian Ocean, J. Geophys. Res. 94, 12301–12326, 1989.
[9] S.K. Eittreim and J.I. Ewing, Midplate tectonics in the Indian Ocean, J. Geophys. Res. 77, 6413–6421, 1972.
[10] J.K. Weissel, R.N. Anderson and C.A. Geller, Deformation of the Indo-Australian plate, Nature 287, 284–291, 1980.
[11] C.A. Geller, J.K. Weissel and R.N. Anderson, Heat transfer and intraplate deformation in the Central Indian Ocean, J. Geophys. Res. 88, 1018–1032, 1983.
[12] J.M. Bull and R.A. Scrutton, Fault reactivation in the Central Indian Ocean Basin and the rheology of the oceanic lithosphere, Nature 344, 855–858, 1990.
[13] J.M. Bull and R.A. Scrutton, Seismic reflection images of intraplate deformation, central Indian Ocean, and their tectonic significance, J. Geol. Soc. London 149, 955–966, 1992.
[14] J.K. Weissel and W.F. Haxby, Predicting seafloor topography from SEASAT altimeter data using isostatic models, Eos, Trans. Am. Geophys. Union 63, 907, 1982.
[15] D.C. McAdoo and D.T. Sandwell, Folding of oceanic lithosphere, J. Geophys. Res. 90, 8563–8568, 1985.
[16] C.A. Stein, S. Cloetingh and R. Wortel, Seasat-derived gravity constraints on stress and deformation in the northeastern Indian Ocean, Geophys. Res. Lett. 16, 823–826, 1989.
[17] R.G. Gordon, C. DeMets and D.F. Argus, Kinematic constraints on distributed deformation in the equatorial Indian Ocean from present motion between the Australian and Indian plates, Tectonics 9, 409–422, 1990.
[18] J.R. Cochran and D.A.V. Stow, Proc. ODP, Init. Rep. 116, 388 pp., 1989.
[19] J.R. Cochran, Himalayan uplift, sea level, and the record of Bengal Fan sedimentation, Proc. ODP, Sci. Results 116, 397–414, 1990.
[20] C.A. Stein, S. Cloetingh and R. Wortel, Kinematics and mechanics of the Indian Ocean diffuse boundary zone, Proc. ODP, Sci. Results 116, 261–278, 1990.
[21] G.D. Karner and J.K. Weissel, Compressional deformation of oceanic lithosphere in the Central Indian Ocean: Why it is where it is, Proc. ODP, Sci. Results 116, 279–290, 1990.
[22] D.A. Wiens, C. DeMets, R.G. Gordon, S. Stein, D. Argus, J.F. Engeln, P. Lundgren, D. Quible, C. Stein, S. Weinstein and D.F. Woods, A diffuse plate boundary model for Indian Ocean tectonics, Geophys. Res. Lett. 12, 429–432, 1985.
[23] C. DeMets, R.G. Gordon and D.F. Argus, Intraplate deformation and closure of the Australian–Antarctica–Africa plate circuit, J. Geophys. Res. 93, 11877–11897, 1988.
[24] C. DeMets, R.G. Gordon and P. Vogt, Location of the Africa–Australia–India triple junction and motion between the Australian and Indian plates: Results from an aeromagnetic investigation of the Central Indian and Carlsberg ridges, Geophys. J. Int., in press, 1994.
[25] R.G. Gordon and C. DeMets, Present-day motion along the Owen Fracture Zone and Dalrymple Trough in the Arabian Sea, J. Geophys. Res. 94, 5560–5570, 1989.
[26] J.Y. Royer, R. Gordon, C. DeMets and P. Vogt, New limits on India/Australia motion since Chron 5 (11 Ma) and implications for lithospheric deformation in the equatorial Indian Ocean, Eos, Trans. Am. Geophys. Union 74, 586, 1993.
[27] Shipboard Scientific Party, ODP Leg 116 site survey, Proc. ODP, Init. Rep. 116, 197–210, 1989.
[28] Y.P. Neprochnov, O.V. Levchenko, L.R. Merklin and V.V. Sedov, The structure and tectonics of the intraplate deformations area in the Indian Ocean, Tectonophysics 156, 89–106, 1988.
[29] N. Chamot-Rooke, F. Jestin, B. de Voogd and Phèdre Working Group, Intraplate shortening in the central Indian Ocean determined from a 2100-km-long seismic reflection profile, Geology 21, 1043–1046, 1993.
[30] C.A. Geller and J.K. Weissel, Preliminary results of the 1980 shipboard investigation of deformation of the Indo-Australian plate, I: Seismic reflection, Eos, Trans. Am. Geophys. Union 62, 404, 1981.
[31] D.G. Moore, J.R. Curray, R.W. Raitt and F.J. Emmel, Stratigraphic–seismic section correlations and implications for Bengal Fan history, Init. Rep. DSDP 22, 403–412, 1974.
[32] J.M. Bull and R.A. Scrutton, Seismic velocities and deep structure from wide-angle reflection data around Leg 116 sites, Proc. ODP, Sci. Results 116, 311–316, 1990.
[33] C.H. Scholz and P.A. Cowie, Determination of total strain from faulting using slip measurements, Nature 346, 837–839, 1990.
[34] J. Walsh, J. Watterson and G. Yielding, The importance of small-scale faulting in regional extension, Nature 351, 391–393, 1991.